Advances in Applied Mathematics and Mechanics
Adv. Appl. Math. Mech., Vol. **8**, No. 2, pp. 213-235

DOI: 10.4208/aamm.2013.m362
April 2016

High-Order Finite Volume Methods for Aerosol Dynamic Equations

Ming Cui[1,2,*], Yanxin Su[2] and Dong Liang[3,2]

[1] *College of Applied Sciences, Beijing University of Technology, Beijing 100124, China*
[2] *School of Mathematics, Shandong University, Jinan 250100, China*
[3] *Department of Mathematics and Statistics, York University, 4700 Keele Street, Toronto, Ontario, M3J 1P3, Canada*

Received 29 September 2013; Accepted (in revised version) 29 January 2015

Abstract. Aerosol modeling is very important to study the behavior of aerosol dynamics in atmospheric environment. In this paper we consider numerical methods for the nonlinear aerosol dynamic equations on time and particle size. The finite volume element methods based on the linear interpolation and Hermite interpolation are provided to approximate the aerosol dynamic equation where the condensation and removal processes are considered. Numerical examples are provided to show the efficiency of these numerical methods.

AMS subject classifications: 65M10, 65M15, 65N10, 65N15

Key words: Aerosol dynamic equation, finite volume method, condensation, removal.

1 Introduction

In recent years, the acid rain, Antarctic ozone hole, the sand storms of Northern China and many heavy industry cities "gray haze", which are relevant to atmospheric aerosols, have aroused widespread concern in society. Aerosol particles have a major effect on climate change and human health. Hence, the research on atmospheric aerosols is attracting more attention, see [7,10,11]. In the study of aerosols, the particles are classified as nuclei mode, accumulation mode and coarse mode according to the grain diameter.

Nuclei mode ($r < 0.05\mu$m, average radius is about 0.005μm): These particles are formed by the nucleation of gases or small liquid particles, such as S, SO_2 which are emitted by factories, and sulfate particles by oxidation in atmosphere. The particle in nuclei mode mostly comes from industry pollution and has highly concentration. Nuclei mode is the

*Corresponding author.
Email: mingcui@bjut.edu.cn (M. Cui), suyanxin163@163.com (Y. X. Su), dliang@mathstat.yorku.ca (D. Liang)

 ©2016 Global Science Press

https://doi.org/10.4208/aamm.2013.m362 Published online by Cambridge University Press

most unstable mode, and usually transformed to accumulation mode by nucleation and coagulation, which is one of the mainly source of particles in accumulation mode.

Accumulation mode ($0.05\mu\text{m} < r < 1.0\mu\text{m}$, average radius is about $0.1\mu\text{m}$): The particles in accumulation mode have weak brown motion, a lower coagulation rate than nuclei mode, and lower dry deposition rate than coarse mode, and can be removed by wet deposition as condensation nucleus of clouds. Accumulation mode is the most stable mode in the three mode. The particles in this mode are the aerosol particles that are harmful to people's health, as they usually have harmful substance, and can be inhaled by lung.

Coarse mode ($r > 1.0\mu\text{m}$, average radius is about $5\mu\text{m}$): Aerosol particles are mainly formed by some natural and artificial factors of atmosphere transport, human industry and agriculture, and pollution of human life. For example, the concentration of aerosol particles will increase rapidly under sandstorm weather environment. But residence time of particles in coarse mode is usually very short, several days or even several hours, and are mainly removed by dry and wet deposition. As the aggravation of environment pollution, the diameter range of aerosol particles in coarse mode is getting bigger.

Usually, we use the distribution function $n(v,t)dv$, which represents the number of particles per unit volume, at time t, with particle volume between v and $v+dv$ to describe the aerosol system mathematically. In fact, the aerosol particle evolution is governed by the different physical-chemical processes.

We introduce the aerosol dynamic equations when the condensation growth process, the coagulation process and removal of the particles are taken into account. In this paper we only deal with such cases, which condensation growth rate and removal of the particles are taken into account in separate. Hence, the aerosol dynamic equations considered in this paper have the following form:

$$\begin{aligned}&\frac{\partial n(v,t)}{\partial t}+\underbrace{\frac{\partial[G(v)n(v,t)]}{\partial v}}_{Condensation}+\underbrace{R(v)n(v,t)}_{Removal}\\&=\underbrace{\frac{1}{2}\int_{V_{\min}}^{v-V_{\min}}\beta(v-u,u)n(v-u,t)n(u,t)du-n(v,t)\int_{V_{\min}}^{V_{\max}}\beta(v,u)n(u,t)du}_{Coagulation},\end{aligned}\tag{1.1}$$

with the boundary and initial conditions:

$$n(V_{\min},t)=0, \qquad t\in[0,T], \tag{1.2a}$$

$$n(v,0)=n^0(v), \qquad v\in[V_{\min},V_{\max}]. \tag{1.2b}$$

In practice, one assumes that the aerosol particle distribution has a nonzero minimal volume $V_{\min}$ and a finite maximal volume $V_{\max}$. Thus, the aerosol dynamic equations are built on a finite volume interval $\Omega=[V_{\min},V_{\max}]$.

Next, we introduce different process of the aerosol dynamic equation.

https://doi.org/10.4208/aamm.2013.m362 Published online by Cambridge University Press

Condensation: Aerosol particles grow by the addition of new material onto particles in the gas phase. Usually, chemical reactions produce condensable materials, and then these volatile materials condense on or evaporate form the existing particles. Several numerical studies have been carried out on the condensation process. The change in the size distribution of particles caused by condensation can be expressed as follows:

$$\frac{\partial n(v,t)}{\partial t}=-\frac{\partial[G(v)n(v,t)]}{\partial v}, \tag{1.3}$$

where $G(v)$ is the particle growth rate due to condensation of particles with volume v.

Coagulation: The governing equation which describes the particle size distribution caused by coagulation is proposed as following:

$$\frac{\partial n(v,t)}{\partial t}=\frac{1}{2}\int_{V_{\min}}^{v-V_{\min}}\beta(v-u,u)n(v-u,t)n(u,t)du-n(v,t)\int_{V_{\min}}^{V_{\max}}\beta(v,u)n(u,t)du. \tag{1.4}$$

Removal: The governing equation which is used to describe the removal of aerosol particles is as follows:

$$\frac{\partial n(v,t)}{\partial t}=-R(v)n(v,t), \tag{1.5}$$

where $R(v)$ is the removal rate of particles due to deposition, gravity and interception and other factors.

In this paper, the units of parameters are v in μm^3, n in $particles/cm^3$, t in h, β in cm^3h^{-1}, G in μm^3h^{-1} and R in μm^3h^{-1}, respectively. According to [20], atmospheric aerosols radius usually ranges from 0.001 to 100μm, thus we can assume that the particle population has a nonzero minimal volume $V_{\min}$ and a finite maximal volume $V_{\max}$. On the other hand, sizes of aerosol particle span orders of magnitude to hundreds μm, the size distribution of particles conforms to the very sharp log-normal distribution in statistic then the distribution function $n(v,t)$ changes fiercely in a small interval, the numerical computation becomes more difficult in the ordinary scales.

Particle sizes span orders of magnitude, and to reveal the particle distribution, the logarithmic coordinates are popular. Similarly to [15, 17], we introduce the logarithmic coordinates. Let

$$x=\ln v,\quad y=\ln u,\quad a=\ln V_{\min},\quad b=\ln V_{\max}, \tag{1.6}$$

then the aerosol dynamic equations (1.1) become

$$\begin{aligned}&\frac{\partial n(x,t)}{\partial t}+e^{-x}\frac{\partial[G(x)n(x,t)]}{\partial x}+R(x)n(x,t)\\&=\frac{1}{2}\int_a^{\ln(e^x-e^a)}\beta n(\ln(e^x-e^y),t)n(y,t)e^y dy-n(x,t)\int_a^b\beta n(y,t)e^y dy, \qquad (1.7a)\\&n(x,0)=n^0(x),\quad n(a,t)=0. \qquad (1.7b)\end{aligned}$$

https://doi.org/10.4208/aamm.2013.m362 Published online by Cambridge University Press

Then the different process (1.3)-(1.5) of the aerosol dynamic equations can be rewritten in logarithmic coordinates:

$$\frac{\partial n(x,t)}{\partial t} = -e^{-x}\frac{\partial[G(x)n(x,t)]}{\partial x}, \tag{1.8a}$$

$$\frac{\partial n(x,t)}{\partial t} = \frac{1}{2}\int_a^{\ln(e^x-e^a)} \beta n(\ln(e^x-e^y),t)n(y,t)e^y dy - n(x,t)\int_a^b \beta n(y,t)e^y dy, \tag{1.8b}$$

$$\frac{\partial n(x,t)}{\partial t} = -R(x)n(x,t). \tag{1.8c}$$

Many numerical methods have been studied to solve the aerosol dynamic equations such as sectional method [6], moment method [2, 9, 19], modal method [1], Monte Carlo method [22] maximum entropy method [5].

Recently, Liang et al. developed a splitting wavelet method [15, 16] and an efficient second-order characteristic finite element method [14].

The finite volume method (FVM) [13], which is also called the generalized difference method, uses a volume integral formulation of the differential equation with a finite partitioning set of volume to discrete the solution. The method has been widely used in computational fluid mechanics because it keeps the mass conservation. A typical finite volume method [3, 4, 21] uses piecewise constant functions as test functions, and to keep the same dimension for the spaces of the trial functions and test functions, two different partitions of the domain are needed, one called primal partition is associated with the trial space and one called dual partition is associated with the test space.

The finite volume methods based on the linear interpolation and Hermite interpolation are taken into account to approximate the aerosol dynamic equation for the condensation and removal processes in this paper.

Compared with second-order characteristic finite element method [14] and and wavelet Galerkin methods [16], the finite volume method we presented in this paper is more efficient and feasible. The wavelet method and the wavelet bases [16] are complex. The numerical results obtained in this paper are of significance in application of the computational aerosol dynamics.

The paper is organized as follows. In Section 2, the finite volume element schemes based on the linear interpolation and Hermite interpolation are presented for non-linear aerosol dynamic equations. In Section 3, numerical experiments for multiple log-normal distributions are further given.

2 Finite volume element schemes

2.1 Basic knowledge of finite volume method

Let Γ be a partition of space interval $[a,b]$ such that

$$\Gamma : a = x_0 < x_1 < x_2 < \cdots < x_n = b, \tag{2.1}$$

https://doi.org/10.4208/aamm.2013.m362 Published online by Cambridge University Press

set element $I_i=[x_{i-1},x_i]$, the space step $h_i=x_i-x_{i-1}$ and midpoint $x_{i+\frac{1}{2}}=\frac{1}{2}(x_i+x_{i+1})$. Then we get the dual partition

$$\Delta: a=x_0<x_{\frac{1}{2}}<x_{\frac{3}{2}}<\cdots<x_{n-\frac{1}{2}}<x_n=b. \tag{2.2}$$

The trial space U_h

The basis function of the piecewise linear element space at the point x_i is:

$$\varphi_i(x)=\begin{cases} 1-\dfrac{x_i-x}{h_i}, & x\in I_i, \\ 1-\dfrac{x-x_i}{h_{i+1}}, & x\in I_{i+1}, \\ 0, & \text{others.} \end{cases} \tag{2.3}$$

The basis functions (for simplicity, here we only consider Hermite interpolating function) of the piecewise cubic element space at the point x_i are:

$$\varphi_i^0(x)=\begin{cases} \left(1-\dfrac{x_i-x}{h_i}\right)^2\left(\dfrac{2(x_i-x)}{h_i}+1\right), & x\in I_i, \\ \left(1-\dfrac{x-x_i}{h_{i+1}}\right)^2\left(\dfrac{2(x-x_i)}{h_{i+1}}+1\right), & x\in I_{i+1}, \\ 0, & \text{others,} \end{cases} \tag{2.4a}$$

$$\varphi_i^1(x)=\begin{cases} (x-x_i)\left(\dfrac{x_i-x}{h_i}-1\right)^2, & x\in I_i, \\ (x-x_i)\left(\dfrac{x-x_i}{h_{i+1}}-1\right)^2, & x\in I_{i+1}, \\ 0, & \text{others.} \end{cases} \tag{2.4b}$$

The test space V_h

Basis function of V_h corresponding to the piecewise linear element space U_h is:

$$\psi_j(x)=\begin{cases} 1, & x\in[x_{j-\frac{1}{2}},x_{j+\frac{1}{2}}], \\ 0, & \text{others.} \end{cases} \tag{2.5}$$

Basis functions of V_h corresponding to the piecewise cubic element space U_h are:

$$\psi_j^0(x)=\begin{cases} 1, & x\in[x_{j-\frac{1}{2}},x_{j+\frac{1}{2}}], \\ 0, & \text{others,} \end{cases} \tag{2.6a}$$

$$\psi_j^1(x)=\begin{cases} x-x_j, & x\in[x_{j-\frac{1}{2}},x_{j+\frac{1}{2}}], \\ 0, & \text{others.} \end{cases} \tag{2.6b}$$

https://doi.org/10.4208/aamm.2013.m362 Published online by Cambridge University Press

2.2 Finite volume element scheme based on linear interpolation (L-FVM)

In the particle size direction, we will take the finite element approximation. Let h_i be the space step and I_i be the mesh of the interval $[a,b]=[V_{\min},V_{\max}]$. Let $\{\varphi_i\}_{i=1}^n$ be a set of basis functions associated with the finite volume space. Let $n_h(x,t)$ be the approximation of $n(x,t)$, then we get the following representation:

$$n_h(x,t)=\sum_{i=1}^{n} n_i(t)\varphi_i(x), \tag{2.7}$$

and the set of time-dependent coefficients

$$n(t)=[n_1(t),n_2(t),\cdots,n_n(t)]^T, \tag{2.8}$$

which will be determined from the dynamics equations.

Let $\Delta t=T/K$ be the time step and time level $t^k=k\Delta t$, $k=0,1,\cdots,K$, where K is a positive integer. We will approximate the solutions of the aerosol dynamic equations at time $t^{k+1}=(k+1)\Delta t$.

We approximate $\partial n_h(t_k)/\partial t$ by

$$\frac{\partial n_h(t_k)}{\partial t}\approx\frac{n_h^k-n_h^{k-1}}{\Delta t}.$$

Then, we can get the linear finite volume fully-discrete scheme for the process of of condensation and removal of the aerosol dynamic equation respectively.

2.2.1 The L-FVM scheme to the process of condensation

For the process of condensation of the aerosol dynamic equation, let n_i^k represents $n(x_i,t^k)$, then we can get the following linear finite volume element schemes:

$$\left(\frac{n_h^k-n_h^{k-1}}{\Delta t},\psi_j(x)\right)=-\left(e^{-x}\frac{\partial\left[G(x)\sum_{i=1}^n n_i^k\varphi_i(x)\right]}{\partial x},\psi_j(x)\right). \tag{2.9}$$

By the representation (2.7), we can have

$$\left(\frac{\sum_{i=1}^n n_i^k\varphi_i(x)-\sum_{i=1}^n n_i^{k-1}\varphi_i(x)}{\Delta t},\psi_j(x)\right)=-\left(e^{-x}\frac{\partial\left[G(x)\sum_{i=1}^n n_i^k\varphi_i(x)\right]}{\partial x},\psi_j(x)\right). \tag{2.10}$$

It can also be written in the following form:

$$\frac{1}{\Delta t}\sum_{i=1}^{n} n_i^k(\varphi_i(x),\psi_j(x))+\sum_{i=1}^{n} n_i^k\left(e^{-x}\frac{\partial[G(x)\varphi_i(x)]}{\partial x},\psi_j(x)\right)=\frac{1}{\Delta t}\sum_{i=1}^{n} n_i^{k-1}(\varphi_i(x),\psi_j(x)), \tag{2.11}$$

then

$$\begin{aligned}&\frac{1}{\Delta t}\sum_{i=1}^{n} n_i^k\int_a^b\varphi_i(x)\psi_j(x)dx+\sum_{i=1}^{n} n_i^k\int_a^b e^{-x}\frac{\partial[G(x)\varphi_i(x)]}{\partial x}\psi_j(x)dx\\ =&\frac{1}{\Delta t}\sum_{i=1}^{n} n_i^{k-1}\int_a^b\varphi_i(x)\psi_j(x)dx.\end{aligned} \tag{2.12}$$

https://doi.org/10.4208/aamm.2013.m362 Published online by Cambridge University Press

For simplicity, introduce two notations of coefficient matrices:

$$A=\Big[\int_a^b e^{-x}\frac{\partial[G(x)\varphi_i(x)]}{\partial x}\psi_j(x)dx\Big]_{1\le i,j\le n}, \tag{2.13a}$$

$$B=\Big[\frac{1}{\Delta t}\int_a^b \varphi_i(x)\psi_j(x)dx\Big]_{1\le i,j\le n}. \tag{2.13b}$$

Consequently, we have that

$$(A+B)n^k=Bn^{k-1},\quad k=1,2,\cdots,K. \tag{2.14}$$

The discrete initial conditions of $n(x,0)=n^0(x)$ is derived by projecting the continuous initial distribution $n^0(x)$ onto the finite-dimensional solution space:

$$n_h^0(x)=\sum_{i=1}^n n_i^0\phi_i(x),\quad n^0=[n_1^0,\cdots,n_n^0]^T.$$

2.2.2 The L-FVM scheme to the process of coagulation

Similarly, we can get the linear finite volume element schemes for the process of coagulation:

$$\begin{aligned}&\Big(\frac{\sum_{i=1}^n n_i^k\varphi_i(x)-\sum_{i=1}^n n_i^{k-1}\varphi_i(x)}{\Delta t},\psi_j(x)\Big)\\ =&\Big(\frac{1}{2}\int_a^{\ln(e^x-e^a)}\beta\sum_{i=1}^n n_i^{k-1}\varphi_i(\ln(e^x-e^y))\sum_{i=1}^n n_i^{k-1}\varphi_i(y)e^y dy,\psi_j(x)\Big)\\ &-\Big(\sum_{i=1}^n n_i^{k-1}\varphi_i(x)\int_a^b\beta\sum_{i=1}^n n_i^{k-1}\varphi_i(y)e^y dy,\psi_j(x)\Big),\end{aligned} \tag{2.15}$$

then,

$$\begin{aligned}&\frac{1}{\Delta t}\sum_{i=1}^n n_i^k(\varphi_i(x),\psi_j(x))-\frac{1}{\Delta t}\sum_{i=1}^n n_i^{k-1}(\varphi_i(x),\psi_j(x))\\ =&\sum_{i=1}^n n_i^{k-1}\sum_{r=1}^n n_r^{k-1}\Big(\frac{1}{2}\int_a^{\ln(e^x-e^a)}\beta e^y\varphi_i(\ln(e^x-e^y))\varphi_r(y)dy,\psi_j(x)\Big)\\ &-\sum_{i=1}^n n_i^{k-1}\sum_{r=1}^n n_r^{k-1}(\varphi_i(x)\int_a^b\beta e^y\varphi_r(y)dy,\psi_j(x)),\end{aligned} \tag{2.16}$$

which means that:

$$\begin{aligned}&\frac{1}{\Delta t}\sum_{i=1}^n n_i^k\int_a^b\varphi_i(x)\psi_j(x)dx-\frac{1}{\Delta t}\sum_{i=1}^n n_i^{k-1}\int_a^b\varphi_i(x)\psi_j(x)dx\\ =&\frac{1}{2}\sum_{i=1}^n n_i^{k-1}\sum_{r=1}^n n_r^{k-1}\int_a^b\int_a^{\ln(e^x-e^a)}\beta e^y\varphi_i(\ln(e^x-e^y))\varphi_r(y)\psi_j(x)dydx\\ &-\sum_{i=1}^n n_i^{k-1}\sum_{r=1}^n n_r^{k-1}\int_a^b\int_a^b\beta e^y\varphi_i(x)\varphi_r(y)\psi_j(x)dydx.\end{aligned} \tag{2.17}$$

https://doi.org/10.4208/aamm.2013.m362 Published online by Cambridge University Press

Introduce the following notations:

$$B=\Big[\frac{1}{\delta t}\int_a^b \varphi_i(x)\psi_j(x)dx\Big]_{1\le i,j\le n}, \tag{2.18a}$$

$$C_j=\Big[\frac{1}{2}\int_a^b\int_a^{\ln(e^x-e^a)} \beta e^y\varphi_i(\ln(e^x-e^y))\varphi_r(y)\psi_j(x)dydx\Big]_{1\le i,r\le n}, \tag{2.18b}$$

$$D_j=\Big[\int_a^b\int_a^b \beta e^y\varphi_i(x)\varphi_r(y)\psi_j(x)dydx\Big]_{1\le i,r\le n}, \tag{2.18c}$$

$$E=\begin{bmatrix} (n^{k-1})^T(C_1-D_1)\\ (n^{k-1})^T(C_2-D_2)\\ \vdots\\ (n^{k-1})^T(C_n-D_n)\end{bmatrix}, \tag{2.18d}$$

where $(n^{k-1})^T$ is the transpose of n^{k-1}. Then (2.17) can be written as the following:

$$Bn^k=(B+E)n^{k-1},\quad k=1,2,\cdots,K. \tag{2.19}$$

The discrete initial conditions of $n(x,0)=n^0(x)$ can also be derived by projecting the continuous initial distribution $n^0(x)$ onto the finite-dimensional solution space as,

$$n_h^0(x)=\sum_{i=1}^n n_i^0\phi_i(x),\quad n^0=[n_1^0,\cdots,n_n^0]^T.$$

2.2.3 The L-FVM scheme to the process of removal

Similarly, the linear finite volume element scheme for aerosol dynamic equation of removal process can be written in the following form:

$$\Big(\frac{\sum_{i=1}^n n_i^k\varphi_i(x)-\sum_{i=1}^n n_i^{k-1}\varphi_i(x)}{\Delta t},\psi_j(x)\Big)=-\Big(R(x)\sum_{i=1}^n n_i^k\varphi_i(x),\psi_j(x)\Big), \tag{2.20}$$

then

$$\frac{1}{\Delta t}\sum_{i=1}^n n_i^k(\varphi_i(x),\psi_j(x))+\sum_{i=1}^n n_i^k(R(x)\varphi_i(x),\psi_j(x))=\frac{1}{\Delta t}\sum_{i=1}^n n_i^{k-1}(\varphi_i(x),\psi_j(x)), \tag{2.21}$$

which means that

$$\begin{aligned}&\frac{1}{\Delta t}\sum_{i=1}^n n_i^k\int_a^b\varphi_i(x)\psi_j(x)dx+\sum_{i=1}^n n_i^k\int_a^b R(x)\varphi_i(x)\psi_j(x)dx\\ =&\frac{1}{\Delta t}\sum_{i=1}^n n_i^{k-1}\int_a^b\varphi_i(x)\psi_j(x)dx.\end{aligned} \tag{2.22}$$

https://doi.org/10.4208/aamm.2013.m362 Published online by Cambridge University Press

Introduce the following notation for the matrices of coefficients:

$$B=\Big[\frac{1}{\Delta t}\int_a^b \varphi_i(x)\psi_j(x)dx\Big]_{1\le i,j\le n}, \tag{2.23a}$$

$$F=\Big[\int_a^b R(x)\varphi_i(x)\psi_j(x)dx\Big]_{1\le i,j\le n}. \tag{2.23b}$$

Finally, we can get

$$(B+F)n^k=Bn^{k-1},\quad k=1,2,\cdots,K. \tag{2.24}$$

The discrete initial conditions of $n(x,0)=n^0(x)$ can also be derived by projecting the continuous initial distribution $n^0(x)$ onto the finite-dimensional solution space as

$$n_h^0(x)=\sum_{i=1}^n n_i^0\phi_i(x),\quad n^0=[n_1^0,\cdots,n_n^0]^T.$$

Based on the above linear finite volume schemes for the process of condensation, coagulation and removal, (1.7) can be computed by:

$$(A+B+F)n^k=(B+E)n^{k-1},\quad k=1,2,\cdots,K, \tag{2.25}$$

and $n^0=[n_1^0,\cdots,n_n^0]^T$.

2.3 Finite volume element Scheme based on Hermite interpolation (H-FVM)

Similar to the L-FVM scheme, we will use the finite volume element approximation based on Hermite interpolation in the size direction. Let h_i be the step and I_i be the mesh of the interval $[a,b]$. Let $\{\varphi_i^p\}_{i=1}^n$ $(p=0,1)$ be a set of basis functions. Then we have the following representation:

$$n_h(x,t)=\sum_{i=0}^n\big(n_i(t)\varphi_i^0(x)+n_i'(t)\varphi_i^1(x)\big), \tag{2.26}$$

and the sets of time-dependent coefficients:

$$n(t)=[n_1(t),n_2(t),\cdots,n_n(t)]^T, \tag{2.27a}$$

$$n'(t)=[n_0'(t),n_1'(t),n_2'(t),\cdots,n_n'(t)]^T. \tag{2.27b}$$

In the time direction, let $\Delta t=T/K$ be the time step and time level $t^k=k\Delta t$, $k=0,1,\cdots,K$, where K is positive integer. We will approximate the solutions of the aerosol dynamic equations at time $t^{k+1}=(k+1)\Delta t$. Let n_i^k and $n_i'^k$ denote $n(x_i,t^k)$ and $n'(x_i,t^k)$ respectively.

Next, we give the H-FVM fully-discrete scheme for aerosol dynamic equation of condensation and removal.

https://doi.org/10.4208/aamm.2013.m362 Published online by Cambridge University Press

2.3.1 The H-FVM scheme to the condensation equation

The H-FVM fully-discrete scheme for aerosol dynamic equation of condensation is as following:

$$\begin{aligned}&\Big(\frac{n_h^k-n_h^{k-1}}{\Delta t},\psi_j^p(x)\Big)\\&=-\Big(e^{-x}\frac{\partial\Big[G(x)\sum_{i=0}^n\big(n_i^k\varphi_i^0(x)+n'^k_i\varphi_i^1(x)\big)\Big]}{\partial x},\psi_j^p(x)\Big),\quad p=0,1.\end{aligned}\tag{2.28}$$

Note that (2.26), we can get

$$\begin{aligned}&\Big(\frac{\sum_{i=0}^n\big(n_i^k\varphi_i^0(x)+n'^k_i\varphi_i^1(x)\big)-\sum_{i=0}^n\big(n_i^{k-1}\varphi_i^0(x)+n'^{k-1}_i\varphi_i^1(x)\big)}{\Delta t},\psi_j^p(x)\Big)\\&=-\big(e^{-x}\frac{\partial\big[G(x)\sum_{i=0}^n\big(n_i^k\varphi_i^0(x)+n'^k_i\varphi_i^1(x)\big)\big]}{\partial x},\psi_j^p(x)\Big),\quad p=0,1.\end{aligned}\tag{2.29}$$

It can also be written in the following form:

$$\begin{aligned}&\frac{1}{\Delta t}\Big(\sum_{i=0}^n\big(n_i^k\varphi_i^0(x)+n'^k_i\varphi_i^1(x)\big),\psi_j^p(x)\Big)+\Big(e^{-x}\frac{\partial\big[G(x)\sum_{i=0}^n(n_i^k\varphi_i^0(x)+n'^k_i\varphi_i^1(x))\big]}{\partial x},\psi_j^p(x)\Big)\\&=\frac{1}{\Delta t}\Big(\sum_{i=0}^n(n_i^{k-1}\varphi_i^0(x)+n'^{k-1}_i\varphi_i^1(x)),\psi_j^p(x)\Big),\quad p=0,1,\end{aligned}\tag{2.30}$$

i.e.,

$$\begin{aligned}&\frac{1}{\Delta t}\Big(\sum_{i=1}^n n_i^k\int_a^b\varphi_i^0(x)\psi_j^p(x)dx+\sum_{i=0}^n n'^k_i\int_a^b\varphi_i^1(x)\psi_j^p(x)dx\Big)\\&+\sum_{i=1}^n n_i^k\int_a^b e^{-x}\frac{\partial[G(x)\varphi_i^0(x)]}{\partial x}\psi_j^p(x)dx+\sum_{i=0}^n n'^k_i\int_a^b e^{-x}\frac{\partial[G(x)\varphi_i^1(x)]}{\partial x}\psi_j^p(x)dx\\&=\frac{1}{\Delta t}\Big(\sum_{i=1}^n n_i^{k-1}\int_a^b\varphi_i^0(x)\psi_j^p(x)dx+\sum_{i=0}^n n'^{k-1}_i\int_a^b\varphi_i^1(x)\psi_j^p(x)dx\Big),\quad p=0,1.\end{aligned}\tag{2.31}$$

For simplicity, introduce the following notations:

$$A^{00}=\Big[\int_a^b e^{-x}\frac{\partial[G(x)\varphi_i^0(x)]}{\partial x}\psi_j^0(x)dx\Big]_{1\le i\le n,1\le j\le n},\tag{2.32a}$$

$$A^{10}=\Big[\int_a^b e^{-x}\frac{\partial[G(x)\varphi_i^1(x)]}{\partial x}\psi_j^0(x)dx\Big]_{0\le i\le n,1\le j\le n},\tag{2.32b}$$

$$A^{01}=\Big[\int_a^b e^{-x}\frac{\partial[G(x)\varphi_i^0(x)]}{\partial x}\psi_j^1(x)dx\Big]_{1\le i\le n,0\le j\le n},\tag{2.32c}$$

$$A^{11}=\Big[\int_a^b e^{-x}\frac{\partial[G(x)\varphi_i^1(x)]}{\partial x}\psi_j^1(x)dx\Big]_{0\le i\le n,0\le j\le n},\tag{2.32d}$$

https://doi.org/10.4208/aamm.2013.m362 Published online by Cambridge University Press

$$B^{00}=\Big[\frac{1}{\Delta t}\int_a^b \varphi_i^0(x)\psi_j^0(x)dx\Big]_{1\le i\le n,1\le j\le n}, \tag{2.32e}$$

$$B^{10}=\Big[\frac{1}{\Delta t}\int_a^b \varphi_i^1(x)\psi_j^0(x)dx\Big]_{0\le i\le n,1\le j\le n}, \tag{2.32f}$$

$$B^{01}=\Big[\frac{1}{\Delta t}\int_a^b \varphi_i^0(x)\psi_j^1(x)dx\Big]_{1\le i\le n,0\le j\le n}, \tag{2.32g}$$

$$B^{11}=\Big[\frac{1}{\Delta t}\int_a^b \varphi_i^1(x)\psi_j^1(x)dx\Big]_{0\le i\le n,0\le j\le n}. \tag{2.32h}$$

Consequently, we have

$$\begin{bmatrix} A^{00} & A^{10} \\ A^{01} & A^{11} \end{bmatrix}\begin{bmatrix} n^k \\ n'^k \end{bmatrix}+\begin{bmatrix} B^{00} & B^{10} \\ B^{01} & B^{11} \end{bmatrix}\begin{bmatrix} n^k \\ n'^k \end{bmatrix}=\begin{bmatrix} B^{00} & B^{10} \\ B^{01} & B^{11} \end{bmatrix}\begin{bmatrix} n^{k-1} \\ n'^{k-1} \end{bmatrix}. \tag{2.33}$$

The discrete initial conditions

$$n_h^0(x)=\sum_{i=1}^n\big(n_i^0\varphi_i^0(x)+n'^0_i\varphi_i^1(x)\big),\quad n_0(t)=0. \tag{2.34}$$

2.3.2 The H-FVM scheme to the process of coagulation

Similarly, the H-FVM fully-discrete scheme for the aerosol dynamic equation of coagulation process can be given by:

$$\begin{aligned}
&\Big(\frac{\sum_{i=0}^n(n_i^k\varphi_i^0(x)+n'^k_i\varphi_i^1(x))-\sum_{i=0}^n(n_i^{k-1}\varphi_i^0(x)+n'^{k-1}_i\varphi_i^1(x))}{\Delta t},\psi_j^p(x)\Big)\\
=&\frac{1}{2}\Big(\int_a^{\ln(e^x-e^a)}\beta\Big[\sum_{i=1}^n n_i^{k-1}\varphi_i^0(\ln(e^x-e^y))+\sum_{i=0}^n n'^{k-1}_i\varphi_i^1(\ln(e^x-e^y))\Big]\\
&\times\Big[\sum_{i=1}^n n_i^{k-1}\varphi_i^0(y)+\sum_{i=0}^n n'^{k-1}_i\varphi_i^1(y)\Big]e^y dy,\psi_j^p(x)\Big)\\
&-\Big(\Big[\sum_{i=1}^n n_i^{k-1}\varphi_i^0(x)+\sum_{i=0}^n n'^{k-1}_i\varphi_i^1(x)\Big]\\
&\times\int_a^b\beta\Big[\sum_{i=1}^n n_i^{k-1}\varphi_i^0(y)+\sum_{i=0}^n n'^{k-1}_i\varphi_i^1(y)\Big]e^y dy,\psi_j^p(x)\Big),\quad p=0,1.
\end{aligned} \tag{2.35}$$

Then, we can get

$$\begin{aligned}
&\frac{1}{\Delta t}\Big(\sum_{i=1}^n n_i^k\int_a^b\varphi_i^0(x)\psi_j^p(x)dx+\sum_{i=0}^n n'^k_i\int_a^b\varphi_i^1(x)\psi_j^p(x)dx\Big)\\
&-\frac{1}{\Delta t}\Big(\sum_{i=1}^n n_i^{k-1}\int_a^b\varphi_i^0(x)\psi_j^p(x)dx+\sum_{i=0}^n n'^{k-1}_i\int_a^b\varphi_i^1(x)\psi_j^p(x)dx\Big)
\end{aligned}$$

https://doi.org/10.4208/aamm.2013.m362 Published online by Cambridge University Press

$$
\begin{aligned}
=&\frac{1}{2}\sum_{i=1}^{n} n_i^{k-1}\sum_{r=1}^{n} n_r^{k-1}\int_a^b\int_a^{\ln(e^x-e^a)} \beta e^y \varphi_i^0(\ln(e^x-e^y))\varphi_r^0(y)\psi_j^p(x)dydx\\
&+\frac{1}{2}\sum_{i=1}^{n} n_i^{k-1}\sum_{r=0}^{n} n'^{k-1}_r\int_a^b\int_a^{\ln(e^x-e^a)} \beta e^y \varphi_i^0(\ln(e^x-e^y))\varphi_r^1(y)\psi_j^p(x)dydx\\
&+\frac{1}{2}\sum_{i=0}^{n} n'^{k-1}_i\sum_{r=1}^{n} n_r^{k-1}\int_a^b\int_a^{\ln(e^x-e^a)} \beta e^y \varphi_i^1(\ln(e^x-e^y))\varphi_r^0(y)\psi_j^p(x)dydx\\
&+\frac{1}{2}\sum_{i=0}^{n} n'^{k-1}_i\sum_{r=0}^{n} n'^{k-1}_r\int_a^b\int_a^{\ln(e^x-e^a)} \beta e^y \varphi_i^1(\ln(e^x-e^y))\varphi_r^1(y)\psi_j^p(x)dydx\\
&-\sum_{i=1}^{n} n_i^{k-1}\sum_{r=1}^{n} n_r^{k-1}\int_a^b\int_a^b \beta e^y \varphi_i^0(x)\varphi_r^0(y)\psi_j^p(x)dydx\\
&-\sum_{i=1}^{n} n_i^{k-1}\sum_{r=0}^{n} n'^{k-1}_r\int_a^b\int_a^b \beta e^y \varphi_i^0(x)\varphi_r^1(y)\psi_j^p(x)dydx\\
&-\sum_{i=0}^{n} n'^{k-1}_i\sum_{r=1}^{n} n_r^{k-1}\int_a^b\int_a^b \beta e^y \varphi_i^1(x)\varphi_r^0(y)\psi_j^p(x)dydx\\
&-\sum_{i=0}^{n} n'^{k-1}_i\sum_{r=0}^{n} n'^{k-1}_r\int_a^b\int_a^b \beta e^y \varphi_i^1(x)\varphi_r^1(y)\psi_j^p(x)dydx,\quad p=0,1.
\end{aligned}
\tag{2.36}
$$

Introduce the following notations

$$B^{00}=\Big[\frac{1}{\Delta t}\int_a^b \varphi_i^0(x)\psi_j^0(x)dx\Big]_{1\le i\le n,1\le j\le n}', \tag{2.37a}$$

$$B^{10}=\Big[\frac{1}{\Delta t}\int_a^b \varphi_i^1(x)\psi_j^0(x)dx\Big]_{0\le i\le n,1\le j\le n}', \tag{2.37b}$$

$$B^{01}=\Big[\frac{1}{\Delta t}\int_a^b \varphi_i^0(x)\psi_j^1(x)dx\Big]_{1\le i\le n,0\le j\le n}', \tag{2.37c}$$

$$B^{11}=\Big[\frac{1}{\Delta t}\int_a^b \varphi_i^1(x)\psi_j^1(x)dx\Big]_{0\le i\le n,0\le j\le n}', \tag{2.37d}$$

$$C_j^{00}=\Big[\frac{1}{2}\int_a^b\int_a^{\ln(e^x-e^a)} \beta e^y \varphi_i^0(\ln(e^x-e^y))\varphi_r^0(y)\psi_j^0(x)dydx\Big]_{1\le i\le n,1\le r\le n}', \tag{2.37e}$$

$$C_j^{10}=\Big[\frac{1}{2}\int_a^b\int_a^{\ln(e^x-e^a)} \beta e^y \varphi_i^1(\ln(e^x-e^y))\varphi_r^0(y)\psi_j^0(x)dydx\Big]_{0\le i\le n,1\le r\le n}', \tag{2.37f}$$

$$C_j^{01}=\Big[\frac{1}{2}\int_a^b\int_a^{\ln(e^x-e^a)} \beta e^y \varphi_i^0(\ln(e^x-e^y))\varphi_r^1(y)\psi_j^0(x)dydx\Big]_{1\le i\le n,0\le r\le n}', \tag{2.37g}$$

$$C_j^{11}=\Big[\frac{1}{2}\int_a^b\int_a^{\ln(e^x-e^a)} \beta e^y \varphi_i^1(\ln(e^x-e^y))\varphi_r^1(y)\psi_j^0(x)dydx\Big]_{0\le i\le n,0\le r\le n}', \tag{2.37h}$$

$$D_j^{00}=\Big[\int_a^b\int_a^b \beta e^y \varphi_i^0(x)\varphi_r^0(y)\psi_j^0(x)dydx\Big]_{1\le i\le n,1\le r\le n}', \tag{2.37i}$$

https://doi.org/10.4208/aamm.2013.m362 Published online by Cambridge University Press

$$D_j^{10}=\left[\int_a^b\int_a^b \beta e^y \varphi_i^1(x)\varphi_r^0(y)\psi_j^0(x)dydx\right]_{0\le i\le n,1\le r\le n}, \tag{2.37j}$$

$$D_j^{01}=\left[\int_a^b\int_a^b \beta e^y \varphi_i^0(x)\varphi_r^1(y)\psi_j^0(x)dydx\right]_{1\le i\le n,0\le r\le n}, \tag{2.37k}$$

$$D_j^{11}=\left[\int_a^b\int_a^b \beta e^y \varphi_i^1(x)\varphi_r^1(y)\psi_j^0(x)dydx\right]_{0\le i\le n,0\le r\le n}, \tag{2.37l}$$

$$M_j^{00}=\left[\frac{1}{2}\int_a^b\int_a^{\ln(e^x-e^a)} \beta e^y \varphi_i^0(\ln(e^x-e^y))\varphi_r^0(y)\psi_j^1(x)dydx\right]_{1\le i\le n,1\le r\le n}, \tag{2.37m}$$

$$M_j^{10}=\left[\frac{1}{2}\int_a^b\int_a^{\ln(e^x-e^a)} \beta e^y \varphi_i^1(\ln(e^x-e^y))\varphi_r^0(y)\psi_j^1(x)dydx\right]_{0\le i\le n,1\le r\le n}, \tag{2.37n}$$

$$M_j^{01}=\left[\frac{1}{2}\int_a^b\int_a^{\ln(e^x-e^a)} \beta e^y \varphi_i^0(\ln(e^x-e^y))\varphi_r^1(y)\psi_j^1(x)dydx\right]_{1\le i\le n,0\le r\le n}, \tag{2.37o}$$

$$M_j^{11}=\left[\frac{1}{2}\int_a^b\int_a^{\ln(e^x-e^a)} \beta e^y \varphi_i^1(\ln(e^x-e^y))\varphi_r^1(y)\psi_j^1(x)dydx\right]_{0\le i\le n,0\le r\le n}, \tag{2.37p}$$

$$N_j^{00}=\left[\int_a^b\int_a^b \beta e^y \varphi_i^0(x)\varphi_r^0(y)\psi_j^1(x)dydx\right]_{1\le i\le n,1\le r\le n}, \tag{2.37q}$$

$$N_j^{10}=\left[\int_a^b\int_a^b \beta e^y \varphi_i^1(x)\varphi_r^0(y)\psi_j^1(x)dydx\right]_{0\le i\le n,1\le r\le n}, \tag{2.37r}$$

$$N_j^{01}=\left[\int_a^b\int_a^b \beta e^y \varphi_i^0(x)\varphi_r^1(y)\psi_j^1(x)dydx\right]_{1\le i\le n,0\le r\le n}, \tag{2.37s}$$

$$N_j^{11}=\left[\int_a^b\int_a^b \beta e^y \varphi_i^1(x)\varphi_r^1(y)\psi_j^1(x)dydx\right]_{0\le i\le n,0\le r\le n}, \tag{2.37t}$$

and

$$E^{00}=\begin{bmatrix} (n^{k-1})^T(C_1^{00}-D_1^{00})+(n'^{k-1})^T(C_1^{10}-D_1^{10}) \\ (n^{k-1})^T(C_2^{00}-D_2^{00})+(n'^{k-1})^T(C_2^{10}-D_2^{10}) \\ \vdots \\ (n^{k-1})^T(C_n^{00}-D_n^{00})+(n'^{k-1})^T(C_n^{10}-D_n^{10}) \end{bmatrix}, \tag{2.38a}$$

$$E^{10}=\begin{bmatrix} (n^{k-1})^T(C_1^{01}-D_1^{01})+(n'^{k-1})^T(C_1^{11}-D_1^{11}) \\ (n^{k-1})^T(C_2^{01}-D_2^{01})+(n'^{k-1})^T(C_2^{11}-D_2^{11}) \\ \vdots \\ (n^{k-1})^T(C_n^{01}-D_n^{01})+(n'^{k-1})^T(C_n^{11}-D_n^{11}) \end{bmatrix}, \tag{2.38b}$$

$$E^{01}=\begin{bmatrix} (n^{k-1})^T(M_0^{00}-N_0^{00})+(n'^{k-1})^T(M_0^{10}-N_0^{10}) \\ (n^{k-1})^T(M_1^{00}-N_1^{00})+(n'^{k-1})^T(M_1^{10}-N_1^{10}) \\ (n^{k-1})^T(M_2^{00}-N_2^{00})+(n'^{k-1})^T(M_2^{10}-N_2^{10}) \\ \vdots \\ (n^{k-1})^T(M_n^{00}-N_n^{00})+(n'^{k-1})^T(M_n^{10}-N_n^{10}) \end{bmatrix}, \tag{2.38c}$$

https://doi.org/10.4208/aamm.2013.m362 Published online by Cambridge University Press

$$E^{11}=\begin{bmatrix} (n^{k-1})^T(M_0^{01}-N_0^{01})+(n'^{k-1})^T(M_0^{11}-N_0^{11}) \\ (n^{k-1})^T(M_1^{01}-N_1^{01})+(n'^{k-1})^T(M_1^{11}-N_1^{11}) \\ (n^{k-1})^T(M_2^{01}-N_2^{01})+(n'^{k-1})^T(M_2^{11}-N_2^{11}) \\ \vdots \\ (n^{k-1})^T(M_n^{01}-N_n^{01})+(n'^{k-1})^T(M_n^{11}-N_n^{11}) \end{bmatrix}, \tag{2.38d}$$

then, we can get

$$\begin{bmatrix} B^{00}B^{10} \\ B^{01}B^{11} \end{bmatrix}\begin{bmatrix} n^k \\ n'^k \end{bmatrix}=\left(\begin{bmatrix} E^{00}E^{10} \\ E^{01}E^{11} \end{bmatrix}+\begin{bmatrix} B^{00}B^{10} \\ B^{01}B^{11} \end{bmatrix}\right)\begin{bmatrix} n^{k-1} \\ n'^{k-1} \end{bmatrix}, \quad k=1,2,\cdots,K. \tag{2.39}$$

2.3.3 The H-FVM scheme to the process of removal

Similarly, we can obtain the H-FVM fully-discrete scheme for aerosol dynamic equation of the removal process in the following form:

$$\begin{aligned} &\left(\frac{\sum_{i=0}^n(n_i^k\varphi_i^0(x)+n'^k_i\varphi_i^1(x))-\sum_{i=0}^n(n_i^{k-1}\varphi_i^0(x)+n'^{k-1}_i\varphi_i^1(x))}{\Delta t},\psi_j^p(x)\right) \\ &=-\left(R(x)\sum_{i=0}^n(n_i^k\varphi_i^0(x)+n'^k_i\varphi_i^1(x)),\psi_j^p(x)\right), \quad p=0,1. \end{aligned} \tag{2.40}$$

Also,

$$\begin{aligned} &\frac{1}{\Delta t}\left(\sum_{i=0}^n(n_i^k\varphi_i^0(x)+n'^k_i\varphi_i^1(x)),\psi_j^p(x)\right)+\left(R(x)\sum_{i=0}^n(n_i^k\varphi_i^0(x)+n'^k_i\varphi_i^1(x)),\psi_j^p(x)\right) \\ &=\frac{1}{\Delta t}\left(\sum_{i=0}^n(n_i^{k-1}\varphi_i^0(x)+n'^{k-1}_i\varphi_i^1(x)),\psi_j^p(x)\right), \quad p=0,1, \end{aligned} \tag{2.41}$$

that is

$$\begin{aligned} &\frac{1}{\Delta t}\left(\sum_{i=1}^n n_i^k\int_a^b\varphi_i^0(x)\psi_j^p(x)dx+\sum_{i=0}^n n'^k_i\int_a^b\varphi_i^1(x)\psi_j^p(x)dx\right) \\ &+\sum_{i=1}^n n_i^k\int_a^b R(x)\varphi_i^0(x)\psi_j^p(x)dx+\sum_{i=0}^n n'^k_i\int_a^b R(x)\varphi_i^0(x)\psi_j^p(x)dx \\ &=\frac{1}{\Delta t}\left(\sum_{i=1}^n n_i^{k-1}\int_a^b\varphi_i^0(x)\psi_j^p(x)dx+\sum_{i=0}^n n'^{k-1}_i\int_a^b\varphi_i^1(x)\psi_j^p(x)dx\right), \quad p=0,1. \end{aligned} \tag{2.42}$$

Denote matrices of coefficients as follows:

$$F^{00}=\left[\int_a^b R(x)\varphi_i^0(x)\psi_j^0(x)dx\right]_{1\le i\le n,1\le j\le n}, \quad F^{10}=\left[\int_a^b R(x)\varphi_i^1(x)\psi_j^0(x)dx\right]_{0\le i\le n,1\le j\le n}, \tag{2.43a}$$

https://doi.org/10.4208/aamm.2013.m362 Published online by Cambridge University Press

$$F^{01}=\Big[\int_a^b R(x)\varphi_i^0(x)\psi_j^1(x)dx\Big]_{1\le i\le n,0\le j\le n},\quad F^{11}=\Big[\int_a^b R(x)\varphi_i^1(x)\psi_j^1(x)dx\Big]_{0\le i\le n,0\le j\le n},\tag{2.43b}$$

$$B^{00}=\Big[\frac{1}{\Delta t}\int_a^b \varphi_i^0(x)\psi_j^0(x)dx\Big]_{1\le i\le n,1\le j\le n},\quad B^{10}=\Big[\frac{1}{\Delta t}\int_a^b \varphi_i^1(x)\psi_j^0(x)dx\Big]_{0\le i\le n,1\le j\le n},\tag{2.43c}$$

$$B^{01}=\Big[\frac{1}{\Delta t}\int_a^b \varphi_i^0(x)\psi_j^1(x)dx\Big]_{1\le i\le n,0\le j\le n},\quad B^{11}=\Big[\frac{1}{\Delta t}\int_a^b \varphi_i^1(x)\psi_j^1(x)dx\Big]_{0\le i\le n,0\le j\le n}.\tag{2.43d}$$

Finally, we have

$$\begin{bmatrix} F^{00} & F^{10} \\ F^{01} & F^{11} \end{bmatrix}\begin{bmatrix} n^k \\ n'^k \end{bmatrix}+\begin{bmatrix} B^{00} & B^{10} \\ B^{01} & B^{11} \end{bmatrix}\begin{bmatrix} n^k \\ n'^k \end{bmatrix}=\begin{bmatrix} B^{00}B^{10} \\ B^{01}B^{11} \end{bmatrix}\begin{bmatrix} n^{k-1} \\ n'^{k-1} \end{bmatrix}.\tag{2.44}$$

The discrete initial conditions can be given by

$$n_h^0(x)=\sum_{i=1}^n\big(n_i^0\varphi_i^0(x)+n'^0_i\varphi_i^1(x)\big).\tag{2.45}$$

3 Numerical experiments

Let $n_i(t)$ be the numerical solution at volume nodes x_i and $n^A(x_i,t)$ be value of the analytical solution. L is the length of the particle size and $h=L/n$ is the particle size step. Δt is the time step. The errors of numerical solutions are measured in l_∞, and l_2, norms defined as:

$$Err_\infty=\frac{\max\limits_i\{|n_i(t)-n^A(x_i,t)|\}}{\max\limits_i\{|n^A(x_i,t)|\}},\tag{3.1a}$$

$$Err_2=\frac{\sqrt{\sum_{i=1}^n\big(n_i(t)-n^A(x_i,t)\big)^2}}{\sqrt{\sum_{i=1}^n\big(n^A(x_i,t)\big)^2}}.\tag{3.1b}$$

The ratios of convergence in size are calculated by

$$Ratio=\log\Big(\frac{Err_{l,h_1}}{Err_{l,h_2}}\Big)\Big[\log\Big(\frac{h_1}{h_2}\Big)\Big]^{-1},\quad l=2,\infty.\tag{3.2}$$

A reference solution can be obtained by finite volume method on the very fine grid and associated with very small time step size if no analytical solution is available.

Example 3.1. For the first experiments, we consider the condensation process that the growth rate is a linear function :

$$G(v)=\sigma_0 v,\quad v\in[0,1],\tag{3.3}$$

https://doi.org/10.4208/aamm.2013.m362 Published online by Cambridge University Press

Table 1: The comparison of errors and ratios in size step for the process of condensation.

	h	$\frac{1}{5}$	$\frac{1}{10}$	$\frac{1}{20}$	$\frac{1}{30}$
L-FVM	Err_2	0.2559	0.0637	0.0161	0.0072
	Ratio	–	2.0052	1.9813	1.9830
	Err_∞	0.2316	0.0561	0.0140	0.0062
	Ratio	–	2.0461	2.0072	1.9899
H-FVM	Err_2	0.0072	4.5006e-04	2.8125e-05	5.5556e-06
	Ratio	–	4.0027	4.0002	4.0000
	Err_∞	0.0072	4.5006e-04	2.8125e-05	5.5555e-06
	Ratio	–	4.0027	4.0002	4.0000

the boundary condition:

$$n(0,t)=0, \quad t\in(0,T], \tag{3.4}$$

the initial condition:

$$n(v,0)=N_t v^2, \quad v\in[0,1], \tag{3.5}$$

where N_t is a constant. The analytical solution is given as

$$n^A(v,t)=N_t v^2\exp(-3\sigma_0 t), \qquad v\in[0,1], \quad t\in(0,T]. \tag{3.6}$$

Take parameters $\sigma_0=1h^{-1}$, $N_t=10\text{particles/cm}^3$. The size steps are $h=1/5,1/10,1/20$ and $1/30$ respectively, the corresponding time steps for L-FVM and H-FVM are $\Delta t=h^2$ and $\Delta t=h^4$, respectively. The comparison of errors and ratios of convergence at time $T=1h$ by L-FVM and H-FVM are shown in Table 1.

The first part in Table 1 shows the numerical results obtained by L-FVM and the second part is obtained by H-FVM at time $T=1h$. It is clearly shown that the numerical solutions are in agreement with the analytic solution in size at time $T=1h$. We can see that L-FVM is of second-order accuracy and H-FVM is of four-order accuracy in size step in both l_∞, and l_2, norm. Moreover, the errors of of H-FVM in l_2, norm is much smaller than those of L-FVM, which means that we can use a large size step to get the high-order approximation by H-FVM while L-FVM must use small size step to get similar error precision.

Example 3.2. In this example, we only consider the aerosol removal process. Let

$$R(v)=R_0 v^{\frac{1}{3}}, \quad v\in[V_{\min},V_{\max}], \tag{3.7}$$

the boundary condition:

$$n(0,t)=0, \quad t\in(0,T], \tag{3.8}$$

and the initial condition:

$$n(v,0)=\frac{N_t}{3\sqrt{2\pi}\ln\sigma}\exp\Big[-\frac{\ln^2(\frac{v}{v_g})}{18\ln^2\sigma}\Big]\frac{1}{v}, \quad v\in[V_{\min},V_{\max}]. \tag{3.9}$$

https://doi.org/10.4208/aamm.2013.m362 Published online by Cambridge University Press

Table 2: The comparison of errors and ratios in size step for the process of removal.

	h	$\frac{1}{5}$	$\frac{1}{10}$	$\frac{1}{15}$	$\frac{1}{20}$
L-FVM	Err_2	0.0028	6.7191e-04	2.9752e-04	1.6732e-04
	Ratio	–	2.0351	2.0092	2.0008
	Err_∞	0.0027	6.5706e-04	2.9074e-04	1.6329e-04
	Ratio	–	2.0350	2.0109	2.0054
H-FVM	Err_2	1.1187e-04	6.9829e-06	1.3792e-06	4.3638e-07
	Ratio	–	4.0019	4.0002	4.0001
	Err_∞	1.1053e-04	6.9308e-06	1.3683e-06	4.3305e-07
	Ratio	–	3.9953	4.0013	3.9991

The analytical solution is given by

$$n^A(v,t)=\frac{N_t}{3\sqrt{2\pi}\ln\sigma}\exp\Big[-\frac{\ln^2(\frac{v}{v_g})}{18\ln^2\sigma}\Big]\frac{1}{v}\exp(-R(v)t),\quad v\in[V_{\min},V_{\max}],\quad t\in(0,T],\tag{3.10}$$

where N_t is a constant, which represents the total initial number of particles, and v_g is the geometric average volume and σ is the standard deviation. In this example, $R_0=1h^{-1}$, $N_t=10^4$particles/cm^3, $v_g=0.1\mu$m^3, $\sigma=1.35\mu$m^3, and $V_{\min}=e^{-7}\mu$m^3, $V_{\max}=e\mu$m^3. Since $V_{\min}$ is much smaller than $V_{\max}$, we convert these equations to logarithmic coordinates:

$$R(x)=R_0e^{\frac{x}{3}},\qquad x\in[\ln V_{\min},\ln V_{\max}],\tag{3.11a}$$

$$n(0,t)=0,\qquad t\in(0,T],\tag{3.11b}$$

$$n(x,0)=\frac{N_t}{3\sqrt{2\pi}\ln\sigma}\exp\Big[-\frac{(x-\ln v_g)^2}{18\ln^2\sigma}\Big]\frac{1}{e^x},\qquad x\in[\ln V_{\min},\ln V_{\max}],\tag{3.11c}$$

$$n^A(x,t)=\frac{N_t}{3\sqrt{2\pi}\ln\sigma}\exp\Big[-\frac{(x-\ln v_g)^2}{18\ln^2\sigma}\Big]\frac{1}{e^x}\exp(-R(x)t),\quad x\in[\ln V_{\min},\ln V_{\max}],\quad t\in(0,T].\tag{3.11d}$$

The size steps are $h=1/5,1/10,1/15$ and $1/20$, the corresponding time steps for L-FVM and H-FVM are $\Delta t=h^2$ and $\Delta t=h^4$.

The comparison of errors and ratios of convergence at time $T=1h$ by the two methods are shown in Table 2. We can see that errors and ratios of convergence of numerical solutions of this example are similar to the result of Example 3.1.

Example 3.3. In this example, we consider a test problem (see [17]), where the coagulation rate $\beta(u,v)$ is a constant and the growth rate $G(v)$ is linear:

$$G(v)=\sigma_0v,\quad \beta(u,v)=\beta_0.\tag{3.12}$$

The initial number distribution is exponential (see [17])

$$n(v,0)=\frac{N_t}{v_m}\exp\Big(-\frac{v}{v_m}\Big),\quad v\in[V_{\min},V_{\max}].\tag{3.13}$$

https://doi.org/10.4208/aamm.2013.m362 Published online by Cambridge University Press

Table 3: The error and ratio of the L-FVM for the process of condensation and coagulation.

	h	$\frac{L}{10}$	$\frac{L}{20}$	$\frac{L}{30}$	$\frac{L}{40}$
L-FVM	Err_2	0.0480	0.0113	0.0051	0.0029
	Ratio	–	2.0925	1.9550	1.9789
	Err_∞	0.0389	0.0105	0.0046	0.0026
	Ratio	–	1.8879	2.0140	2.0319

The analytical solution is given by:

$$n^A(v,t)=\frac{4N_t}{v_m(N_t\beta_0 t+2)^2}\exp\Big(-\frac{2v\exp(-\sigma_0 t)}{v_m(N_t\beta_0 t+2)}-\sigma_0 t\Big),\quad v\in[V_{\min},V_{\max}],\quad t\in(0,T],\tag{3.14}$$

where N_t is the initial number of aerosol particles and v_m is the initial mean volume. The corresponding parameters are $\beta_0=2.166\times10^{-7}\text{cm}^3h^{-1}\text{particles}^{-1}$, $\sigma_0=0.3h^{-1}N_t=10^4\text{particles}$, $v_m=0.03\mu\text{m}^3$, $V_{\min}=e^{-7}\mu\text{m}^3$ and $V_{\max}=1\mu\text{m}^3$.

In this example, we choose $n=10$, 20, 30 and 40 and let $L=V_{\max}-V_{\min}$, then the corresponding size step $h=L/n$ and the time step $\Delta t=1/800$. Results of error and ratio of convergence of the L-FVM at time $T=1h$ are listed in Table 3.

It is shown that the linear finite volume scheme for the process of condensation and coagulation is of second-order accuracy in both l_∞ and l_2 norm. We can find that the linear finite volume scheme is efficient to deal with the process of condensation and coagulation.

Example 3.4. We consider a real size distribution problem which describes the effect of a wet removal process. The size distribution of ambient poly-dispersed aerosol can be represented by log-normal distribution function [18].

$$n(d,0)=\frac{N_0}{3\sqrt{2\pi}\ln\sigma_d}\exp\Big[-\frac{\ln^2(d/d_g)}{18\ln^2\sigma_d}\Big]\frac{1}{d},\quad d\in[d_{\min},d_{\max}],\tag{3.15}$$

where N_0 is the total particle number concentration of particles, d_g the initial geometric average particle diameter, and σ_d the geometric standard deviation. The scavenging coefficient $R(d)$ expressing the rate of scavenged aerosols by raindrop is as follows:

$$R(d)=\int_0^\infty K(d,D)E(d,D)dD,\tag{3.16}$$

where

$$K(d,D)=\frac{\pi D^2}{4}U(D)n_R(D),\tag{3.17a}$$

$$E(d,D)=2\Big(\frac{\sqrt{3}\pi}{4}\Big)^{2/3}\Big(\frac{(1-\alpha)(3\sigma+4)}{J+\sigma K}\Big)^{1/3}\Big(\frac{3\pi\mu_a U(D)}{2(1.664)k_bT\lambda}\Big)^{-2/3}d^{-4/3},\tag{3.17b}$$

https://doi.org/10.4208/aamm.2013.m362 Published online by Cambridge University Press

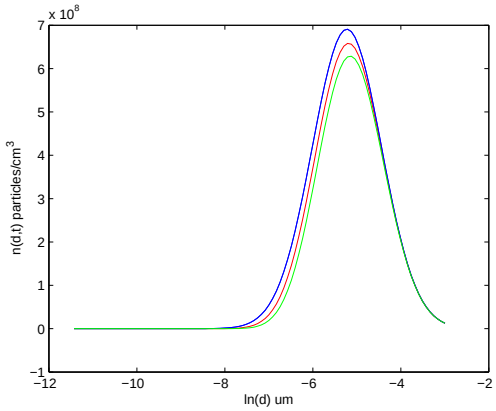


Figure 1: The evolution of precipitated particle size distribution due to wet scavenging in different time: $t=0h$ (blue), $t=1h$ (red), $t=2h$ (green).

where $K(d,D)$ is the collision kernel, and $E(d,D)$ is the collision efficiency, and D is the water droplet diameter, $U(D)$ is the velocity of falling water droplet, $n_R(D)$ is the raindrop size distribution, α is the volume fraction of drop, μ_a is the viscosity of the air, k_b is the Boltzmann's constant ($=1.38\times10^{-23}JK^{-1}$) and T is the temperature of air, λ is the mean free path length of molecules.

$$U(D)=130D^{1/2}. \tag{3.18}$$

The raindrop size distribution is also assumed to have a log-normal distribution in wet scavenging process

$$n_R(D)=\frac{N_t}{3\sqrt{2\pi}\ln\sigma_D}\exp\Big[-\frac{\ln^2(D/D_g)}{18\ln^2\sigma_D}\Big]\frac{1}{D}, \tag{3.19a}$$

$$J=1-6/5\alpha^{1/3}+1/5\alpha^2,\quad K=1-9/5\alpha^{1/3}+\alpha+1/5\alpha^2,\quad \sigma=\mu_w/\mu_a, \tag{3.19b}$$

where N_t is a constant which represents the total initial number of raindrop, D_g is the geometric average volume and σ_d is the standard deviation, μ_w is the viscosity of the raindrop; $N_0=10^7$, $d_{\max}=0.05\mu$m, $d_{\min}=10^{-5}\mu$m, $d_g=0.01\mu$m, $\alpha=5\times10^{-5}$, $T=296.15$K, $\lambda=6.73\times10^{-8}$m, $\mu_a=1.83\times10^{-5}$kgm^{-1}s^{-1}, $\mu_w=9.95\times10^{-4}$kgm^{-1}s^{-1}.

The evolution of precipitated particle size distribution for the parameter $N_t=500$, $\sigma_D=1.5$, $D_g=0.5$mm in different time $t=0h$, $t=1h$, $t=2h$ is shown in Fig. 1. It can be found that the falling velocity of the fine particles is faster for the range of the particle diameter of $<e^{-5}\mu$m. This is consistent with the fact that fine particles can be collected by rain drop through the Brownian diffusion [7].

The impact of the precipitated particle size distribution on the distribution of the rain drops with the parameters $N_t=500$, $\sigma_D=1.5$, $D_g=0.5$mm are shown in Figs. 2-4. The falling efficiency of the precipitated particle decreases when one of parameters N_t, D_g, σ_d gets small and the other two parameters are fixed.

https://doi.org/10.4208/aamm.2013.m362 Published online by Cambridge University Press

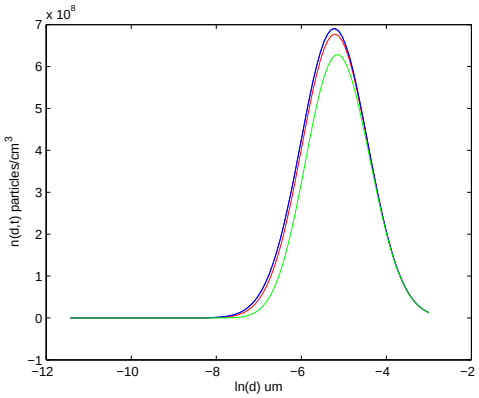


Figure 2: The evolution of precipitated particle size distribution due to wet scavenging for different N_t: $t=0h$ (blue), $N_t=100$ (red, $t=2h$), $N_t=500$ (green, $t=2h$).

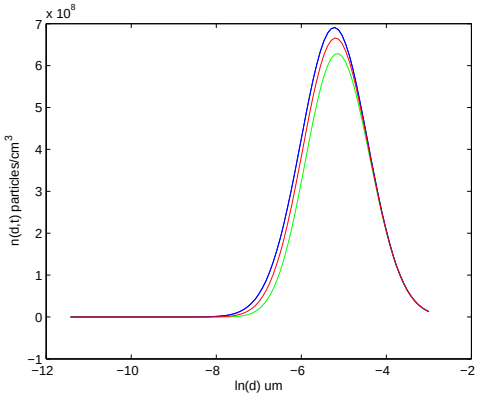


Figure 3: The evolution of precipitated particle size distribution due to wet scavenging for different σ_D: $t=0h$ (blue), $\sigma_D=1.3$ (red, $t=2h$), $\sigma_D=1.5$ (green, $t=2h$).

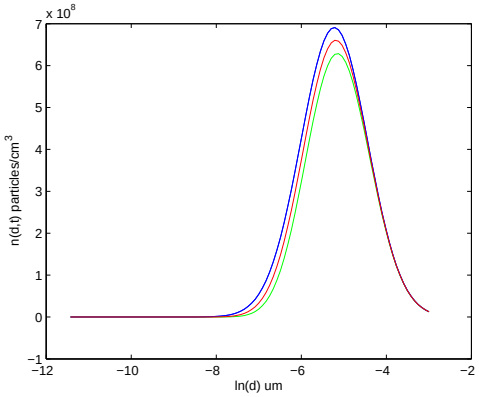


Figure 4: The evolution of precipitated particle size distribution due to wet scavenging for different D_g: $t=0h$ (blue), $D_g=0.3$mm (red, $t=2h$), $D_g=0.5$mm (green, $t=2h$).

https://doi.org/10.4208/aamm.2013.m362 Published online by Cambridge University Press

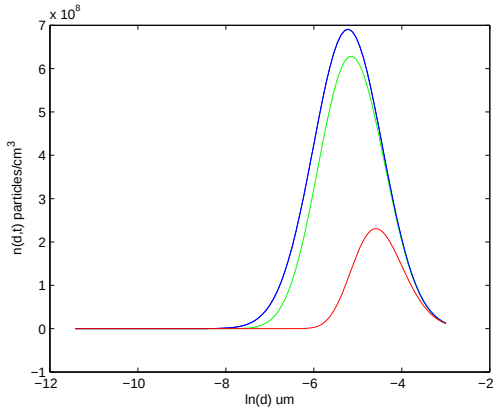


Figure 5: For the same mass of raindrop, the evolution of precipitated particle size distribution due to wet scavenging for different σ_D: $t=0h$ (blue), $\sigma_D=1.3$ (red, $t=2h$), $\sigma_D=1.5$ (green, $t=2h$).

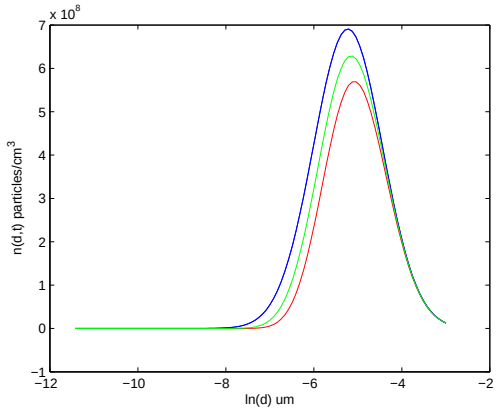


Figure 6: For the same mass of raindrop, the evolution of precipitated particle size distribution due to wet scavenging for different D_g: $t=0h$ (blue), $D_g=0.3$mm (red, $t=2h$), $D_g=0.5$mm (green, $t=2h$).

Fig. 5 and Fig. 6 show that aerosols are scavenged more effectively by raindrops distribution with small D_g than the raindrops with large D_g, for the case of the same mass of raindrops. The figures also show that aerosols are collected more efficiently by raindrops with small σ_d than raindrops with large σ_d. This result agrees well with the existing the theories and experimental data [8] that smaller diameter raindrops have higher collision efficiency, as for the same mass of raindrops, the smaller raindrops will have an increased surface area, which lead to the collision efficiency increase (see [8,9]).

Acknowledgements

M. Cui was supported partly by National Natural Science Foundation of China (Grant No. 11201265 and No. 91430216) and Shandong Natural Science Foundation (Grant

https://doi.org/10.4208/aamm.2013.m362 Published online by Cambridge University Press

No. ZR2012AM003). D. Liang was supported partly by Natural Sciences and Engineering Research Council of Canada and by the National Natural Science Foundation of China under grant No. 11271232.

References

[1] I. J. ACKERMANN, H. HASS, M. MEMMESHEIMER, A. EBEL, F. S. BINKOWSKI AND F. SHANKAR, *Modal aerosol dynamics model for Europe: development and first applications*, Atmos. Environ., 32 (1998), pp. 2981–2999.
[2] J. R. BROCK, J. OATES, AND J. H. SEINFELD, *Moment simulation of aerosol evaporation*, J. Aerosol Sci., 18 (1987), pp. 59–64.
[3] Z. CAI, J. MANDEL AND S. MCCORMICK, *The finite volume element method for diffusion equations on general triangulations*, SIAM J. Numer. Anal., 28 (1991), pp. 392–403.
[4] S. H. CHOU AND Q. LI, *Error estimates in L^2, H^1 and L^1 in covolume methods for elliptic and parabolic problems, a unified approach*, Math. Comput., 69 (2000), pp. 103–120.
[5] A. ELAGARAYHI, *Solution of the dynamic equation of aerosols by means of maximum entropy technique*, J. Quant. Spectrosc. Ra., 75 (2002), pp. 1–11.
[6] F. GERBARD, Y. TAMBOUR AND J. H. SEINFELD, *Sectional representation for simulating aerosol dynamics*, J. Colloid Inter. Sci., 76 (1980), pp. 541–556.
[7] C. H. JUNG, Y. P. KIM, K. W. LEE AND J. H. SEINFELD, *Simulation of the influence of coarse mode particles on the properties of fine mode particles*, J. Aerosol Sci., 33 (2002), pp. 1201–1216.
[8] C. H. JUNG, Y. P. KIM AND K. W. LEE, *Analytic solution for polydispersed aerosol dynamics by a wet removal process*, J. Aerosol Sci., 33 (2002), pp. 753–767.
[9] C. H. JUNG, Y. P. KIM AND K. W. LEE, *A moment model for simulating raindrop scavenging of aerosols* , J. Aerosol Sci., 34 (2003), pp. 1217–1233.
[10] J. KIM, C. H. JUNG, B. C. CHOI, S. N. OH, F. J. BRECHTEL, S. C. YOON, S. W. KIM, *Number size distribution of atmospheric aerosols during ACE-Asia dust and precipitation events,* Atmos. Environ., 41 (2007), pp. 4841–4855.
[11] K. W. LEE, H. CHEN, AND J. A. GIESEKE, *Log-normally preserving size distribution for Brownian coagulation in the free-molecule regime*, Aerosol Sci. Tech., 3 (1984), pp. 53–62.
[12] K. W. LEE, L. A. CURTIS AND H. CHEN, *An analytic solution to free molecule aerosol coagulation*, Aerosol Sci. Tech., 12 (1990), pp. 457–462.
[13] R. LI, Z. CHEN AND W. WU, Generalized Difference Methods for Differential Equations: Numerical Analysis of Finite Volume Methods, Marcel Dekker, 2000.
[14] D. LIANG, W. WANG AND Y. CHENG, *An efficient second-order characteristic finite element method for non-linear aerosol dynamic equations*, Int. J. Numer. Meth. Eng., 80 (2009), pp. 338–354.
[15] D. LIANG, Q. GUO AND S. GONG, *A new splitting wavelet method for solving the general aerosol dynamics equations*, J. Aerosol Sci., 39 (2008), pp. 467–487.
[16] D. LIANG, Q. GUO AND S. GONG, *Wavelet Galerkin methods for aerosol dynamic equations in atmosheric environment*, Commun. Comput. Phys., 6 (2009), pp. 109–130.
[17] A. SANDU AND C. BORDEN, *A framework for the numerical treatment of aerosol dynamics*, Appl. Numer. Math., 45 (2003), pp. 475–497.
[18] J. H. SEINFELD AND S. N. PANDIS, Atmospheric Chemistry and Physics, New York, USA, Wiley, 1998.

https://doi.org/10.4208/aamm.2013.m362 Published online by Cambridge University Press

[19] Y. SEO AND J. R. BROCK, *Distribution for moment simulation of aerosol evaporation*, J. Aerosol Sci., 4 (1990), pp. 511–514.
[20] K. T. WHITBY, *The physical characteristics of sulfur aerosols* , Atmos. Environ., 12 (1978), pp. 135–159.
[21] X. YE, *On the relationship between finite volume and finite element methods applied to the Stokes equations*, Numer. Method PDE, 17 (2001), pp. 440–453.
[22] H. ZHAO AND C. ZHENG, *Monte Carlo sulution of wet removal of aerosols by precipitation*, Atmos. Environ., 40 (2006), pp. 1510–1525.

https://doi.org/10.4208/aamm.2013.m362 Published online by Cambridge University Press